

Global Cross-Modal Geo-Localization: A Million-Scale Dataset and a Physical Consistency Learning Framework

Yutong Hu, Jinhui Chen, Chaoqiang Xu, Yuan Kou, Sili Zhou, Shaocheng Yan, Pengcheng Shi, Qingwu Hu, Jiayuan Li

Abstract—Cross-modal Geo-localization (CMGL) matches ground-level text descriptions with geo-tagged aerial imagery, which is crucial for pedestrian navigation and emergency response. However, existing researches are constrained by narrow geographic coverage and simplistic scene diversity, failing to reflect the immense spatial heterogeneity of global architectural styles and topographic features. To bridge this gap and facilitate universal positioning, we introduce CORE, the first million-scale dataset dedicated to global CMGL. CORE comprises 1,034,786 cross-view images sampled from 225 distinct geographic regions across all continents, offering an unprecedented variety of perspectives in varying environmental conditions and urban layouts. We leverage the zero-shot reasoning of Large Vision-Language Models (LVLMs) to synthesize high-quality scene descriptions rich in discriminative cues. Furthermore, we propose a physical-law-aware network (PLANET) for cross-modal geo-localization. PLANET introduces a novel contrastive learning paradigm to guide textual representations in capturing the intrinsic physical signatures of satellite imagery. Extensive experiments across varied geographic regions demonstrate that PLANET significantly outperforms state-of-the-art methods, establishing a new benchmark for robust, global-scale geo-localization. The dataset and source code will be released at <https://github.com/YtH0823/CORE>.

Index Terms—Geo-localization benchmark, cross-modal, vision-language model, text-to-image retrieval

I. INTRODUCTION

THE advancement of geo-spatial artificial intelligence (GeoAI) is profoundly deepening human’s understanding of the physical world. As a fundamental task within this domain, geo-localization enables the determination of real-time coordinates for ground observation points in GNSS-denied environments, which is critical for applications such as pedestrian navigation [1] and robot localization [2]. Traditional geo-localization methods primarily rely on Cross-View Geo-localization (CVGL). CVGL achieves positioning by performing cross-view retrieval between ground-level imagery and

geo-tagged satellite images, a technique that has already seen widespread adoption [3]–[9]. However, CVGL necessitates the provision of real-time ground images from the query side. In certain restricted environments, capturing and uploading images can be impractical, thereby limiting the operational scope of such positioning systems. To enhance flexibility, recent researches [10], [11] have begun exploring Cross-Modal Geo-localization (CMGL) based on natural language. CMGL directly matches descriptive text of ground scenes with satellite imagery, offering significant value in real-world scenarios. For instance, taxi drivers frequently determine locations based on passengers’ verbal descriptions [12]. Similarly, in emergency calls, individuals seeking help often can only describe their surroundings through language. CMGL leverages this textual information for precise localization, which is of vital importance for improving the efficiency of emergency response [13].

Images from diverse geographic regions exhibit significant visual discrepancies that inevitably induce corresponding divergences in textual descriptions, resulting in a spatial heterogeneity that renders worldwide CMGL an exceptionally challenging task. This divergence stems from two primary factors. From a natural perspective, varying climatic conditions across latitudes result in diverse topographic features [14]. From a humanistic perspective, historical and cultural differences lead to distinct architectural styles. To ensure the global generalization of the model, learning from diverse global imagery is essential [15]. Furthermore, to achieve fine-grained visual-semantic alignment, the model must be trained on exhaustive descriptions of ground scenes, which imposes strict standards on both datasets and methodologies. Although some researches try to promote global-scale localization [11], [16], there remains deficiencies in data volume and modal diversity.

As shown in Table I, existing popular datasets [10], [11], [16]–[23], are flawed in scale and geographic coverage. The lack of text annotations [17]–[23] also prevents them from supporting CMGL tasks. Although some datasets [10], [11], [16] includes textual descriptions, their data collection is limited. To address this scarcity, we introduce a first-ever dataset for Cross-modal geo-localization across worldwide rEGions (CORE), which contains 1,034,786 cross-view image pairs from 225 diverse locations globally. Each ground-level image is paired with a fine-grained textual annotation. Compared with existing datasets, CORE stands out through its vast geographic diversity. This advantage allows it to better

Manuscript received xxx xx, xxxx; revised xxxx xx, xxxx. This work was supported in part by the Xiong’an New Area Science and Technology Innovation Special Program under Grant 2025XAGG0042, in part by the National Natural Science Foundation of China (NSFC) under Grant 42271444, and in part by the Postdoctoral Fellowship Program of CPSF under Grant Number GZB20250065. (Corresponding author: Jiayuan Li.)

Yutong Hu, Jinhui Chen, Chaoqiang Xu, Shaocheng Yan, Pengcheng Shi, Qingwu Hu and Jiayuan Li are with the School of Remote Sensing and Information Engineering, Wuhan University, Wuhan 430079, China, (e-mail: yutonghu@whu.edu.cn; ljiy_wuhu_2012@whu.edu.cn).

Yuan Kou and Sili Zhou are with the First Surveying and Mapping Institute of Hunan province, Changsha 421001, China.

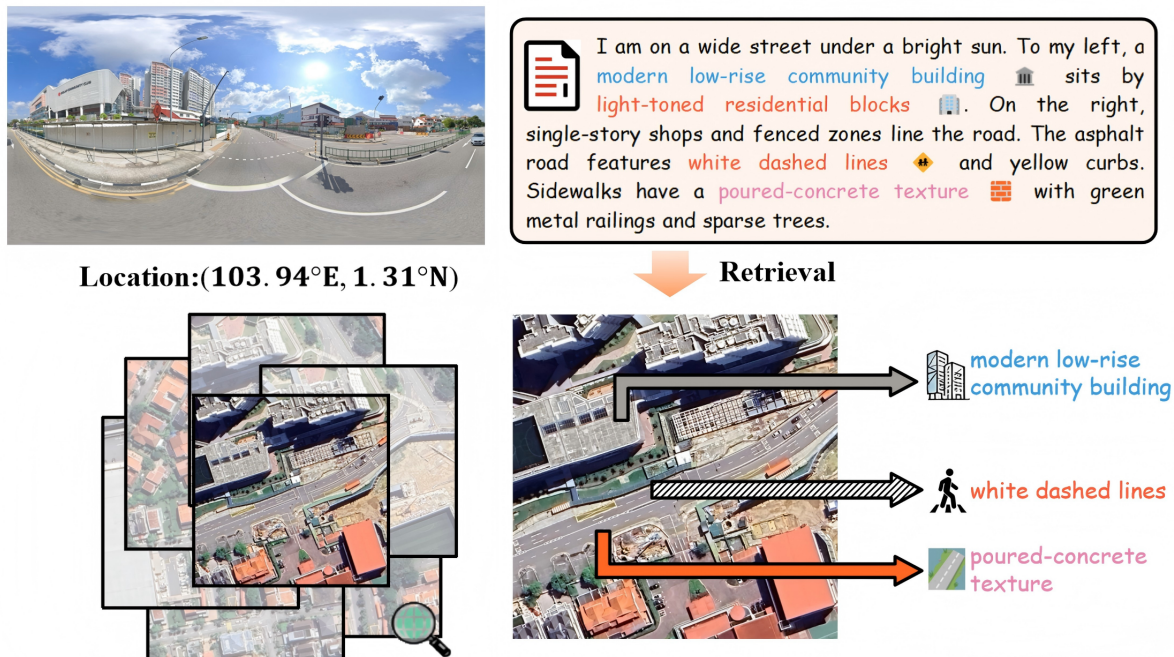


Fig. 1. Illustration of cross-modal geo-localization. This task retrieves satellite imagery based on text queries of the ground environment for position localization. The physical attribute information presented in the text description can yield valuable clues regarding the location.

TABLE I

COMPARISON OF THE CORE DATASET WITH OTHER GEO-LOCALIZATION DATASETS. THE COMPARISON INCLUDES THE NUMBER OF REFERENCE AND QUERY IMAGES, TEXT ANNOTATIONS, DISTRIBUTION RANGE, AND SAMPLING ENVIRONMENT.

Dataset	Query Image	Reference Image	Total Image	Text Annotation	Distribution	Environment
CVGL						
CVUSA [17]	44,416	44,416	88,832	×	USA	Suburban
CVACT [18]	128,334	128,334	256,668	×	Canberra	Urban
VIGOR [19]	90,618	105,214	195,832	×	USA	Urban
University-1652 [20]	50,218	55,227	105,445	×	Campus	Urban
CVGlobal [21]	134,233	134,233	268,466	×	Global (7 regions)	Urban
CV-Cities [22]	223,736	223,736	447,472	×	Global (16 regions)	Urban
DReSS [23]	422,760	174,934	597,694	×	Global (8 regions)	Urban and Suburban
CMGL						
Geotext-1652 [10]	50,218	55,227	105,445	✓	Campus	Urban
CVG-Text [11]	39,792	79,584	119,376	✓	3 Cities	Urban and Suburban
GeoLoc [16]	52,684	105,362	158,052	✓	Global (36 regions)	Urban and Suburban
CORE (Ours)	517,393	517,393	1,034,786	✓	Global (225 regions)	Urban and Suburban

*Note: CVG-Text covers New York, Brisbane, and Tokyo.

meet the requirements for complex scene perception in global navigation. In short, CORE offers comprehensive advantages and notable merits over existing geo-localization datasets.

The essence of CMGL lies in the cross-modal retrieval between ground descriptions and aerial imagery. Its primary goal is to establish semantic associations within a unified latent space. However, existing image-text retrieval methods [24]–[28] predominantly rely on traditional contrastive learning paradigms, which only optimize the global similarity between feature vectors [29]. While these methods can align macroscopic semantics, they struggle to capture the inherent

fine-grained physical attributes within images through coarse-grained global matching. As illustrated in Fig.1, physical attributes such as color, spatial structure, and texture are regularly reflected in the pixel distribution of images and are transformed into semantic cues embedded in the text during scene description. To establish a fine-grained mapping between textual semantics and underlying image attributes, we propose a physical-law-aware network (PLANET). Specifically, PLANET introduces a novel contrastive learning paradigm, which utilizes physical semantic projectors to map textual representations into fine-grained physical attribute de-

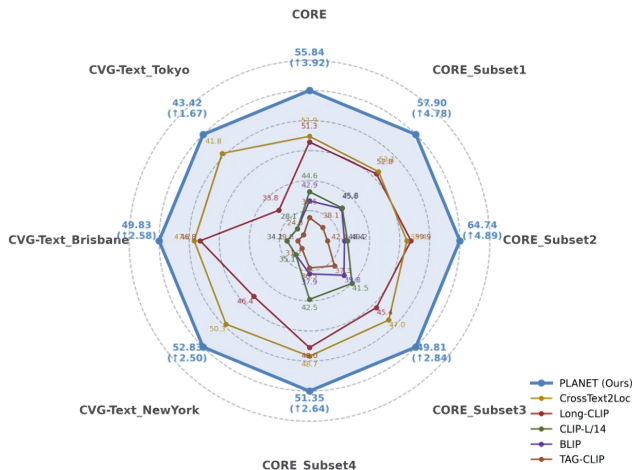


Fig. 2. We evaluate representative methods on the CORE dataset and existing datasets, with PLANET achieving state-of-the-art performance on 8 settings, demonstrating strong localization capabilities. All results are reported as R@1.

scriptors. On the image side, rather than relying on black-box deep features prone to domain bias, we extract a series of deterministic, parameter-free intrinsic physical signatures by decoupling the statistical distribution patterns of the images [30], [31]. These classic heuristic signatures explicitly characterize surface morphology and optical features, serving as robust and unbiased anchors for cross-modal alignment. By explicitly associating textual physical attribute descriptors with these intrinsic physical representations, text branches can be effectively driven to learn and model geographical prior constraints in different environments. This alignment mechanism endows textual features with a high degree of environmental-discriminative power consistent with images, promoting stronger convergence of cross-modal representations within the same environment in the manifold space. By enhancing the feature’s ability to perceive environmental heterogeneity, PLANET fundamentally improves its localization robustness in complex scenes.

We conduct extensive experiments across diverse datasets and geographical settings. The quantitative results presented in Fig. 2 indicate that our proposed PLANET outperforms established methods [11], [24], [25], [27], [32] across various regions of the CORE dataset and other datasets. In summary, the CORE dataset and the PLANET framework aim to establish a large-scale benchmark for CMGL on a global scale. This benchmark will facilitate the development of new algorithms. Our contributions can be summarized as follows:

(1) We propose CORE, the first million-level dataset for the global-scale CMGL task. Encompassing 1,034,786 multi-view images with corresponding fine-grained text annotations across 225 representative geographic regions, CORE bridges existing data gaps through its diverse scene representations.

(2) A physical-law-aware network (i.e., PLANET) is proposed to address the heterogeneity of geographical distribution. By introducing a consistency contrastive learning paradigm, this network can accurately mine potential semantic

cues in text and explicitly align them with the inherent essential attributes of images, significantly enhancing the model’s feature discrimination ability.

(3) Utilizing the CORE dataset, we construct a worldwide CMGL Benchmark to assess large-scale geo-localization under geographic variability. Experimental results indicate that PLANET achieves state-of-the-art performance on this benchmark. Furthermore, we demonstrate the benchmark’s effectiveness in evaluating model adaptation to shifts in geographic distribution through cross-domain generalization experiments.

II. RELATED WORK

In this section, we first discuss existing datasets for geo-localization. Subsequently, we review current localization methods and potential methods derived from the field of text-image retrieval.

A. Geo-localization Datasets

As illustrated in Table 1, geo-localization datasets can be categorized into cross-view and cross-modal geo-localization datasets based on the modal of the query data (e.g., images or text) used for retrieval.

1) *CVGL Datasets*: Over the past decade, a multitude of datasets has been curated to advance the field of cross-view geo-localization. CVUSA [17] initially established a large-scale repository of ground and aerial imagery across the United States; its widely adopted version is a refined subset consisting of 35,532 training and 8,884 testing pairs. Following a similar paradigm, CVACT [18] provides extensive data splits, offering robust empirical support for model evaluation. The VIGOR dataset [19], comprising 105,214 ground images and 90,618 aerial images, further advances the field by relaxing the rigid center-alignment assumption, allowing query points to be stochastically distributed within target regions.

Although these datasets successfully simulate realistic scenarios, their data collection is confined to a single nation, which inherently limits the model’s ability to generalize across the vast geographic domain gaps arising from variations in climate, vegetation, and architectural styles. While CVGlobal [21], CV-Cities [22], and DReSS [23] attempt to broaden the scope by sampling across multiple international cities, the inherent spatial sparsity and discontinuous distribution of their data points fail to capture the statistical complexity of global geographic features, thereby falling short of supporting true worldwide geo-localization. University-1652 [20] provides imagery covering 1,652 groups of satellite and simulated drone images across 72 university campuses worldwide. However, a single campus environment is too limited to support the requirements for large-scale geo-localization. In summary, existing cross-view datasets are insufficient in both data scale and geographic diversity to support true worldwide geo-localization. Furthermore, the reliance on a single visual modality fails to meet the practical multi-modal interaction requirements of pedestrians, tourists, and other end-users.

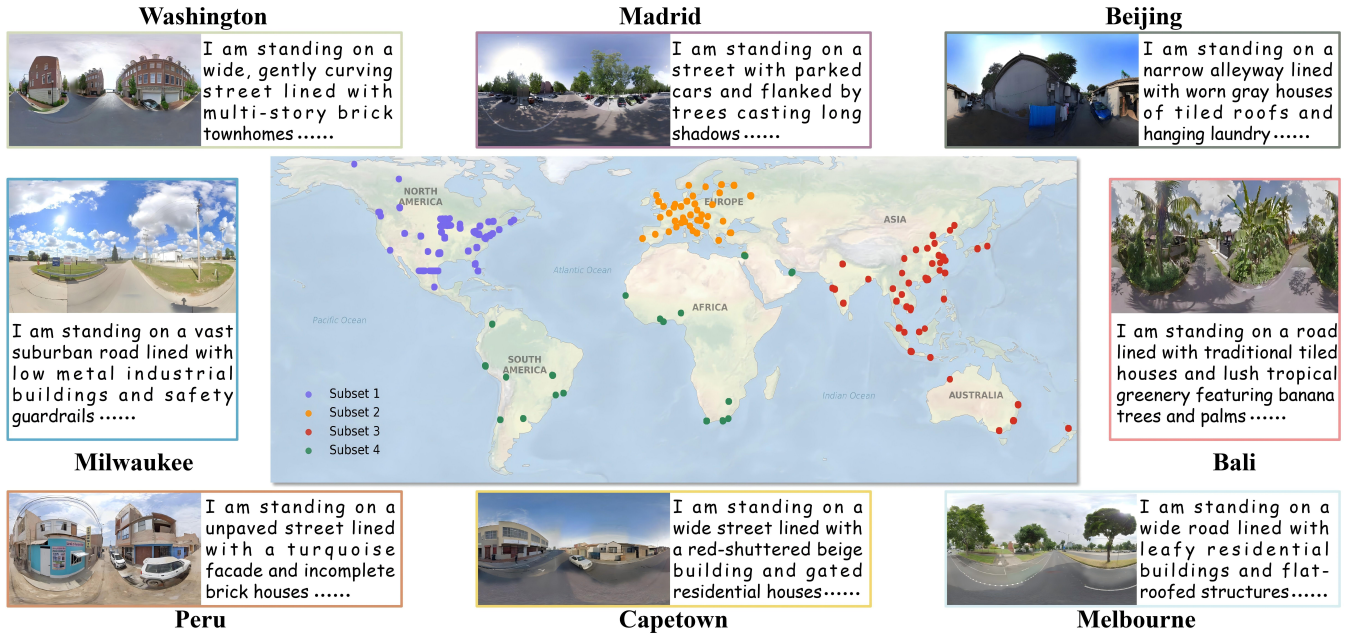


Fig. 3. Geographical distribution map of sampled images and corresponding text annotations from the CORE dataset. CORE exhibits unprecedented global scale and spatial heterogeneity. This extensive diversity ensures a comprehensive representation of varying urban and suburban environments worldwide.

2) *CMGL Datasets*: The evolution of Large Language Models (LLMs) has made it feasible to equip ground-level imagery with precise textual annotations [33]–[36]. To address specific scenarios with high demands for natural language interaction, such as urban navigation [37] and emergency response [38], researchers have developed cross-modal geolocalization datasets pairing text with satellite imagery. However, as illustrated in Table 1, only two publicly available datasets are specifically designed for the Cross-modal Geolocalization task, posing a significant constraint on the advancement of this field.

Geotext-1652 Dataset: Chu et al. [10] proposed the pioneering CMGL dataset tailored for drone navigation. By augmenting UAV images from the image-based University-1652 with global textual descriptions, this dataset effectively extends the benchmark into the cross-modal domain. However, the dataset has certain limitations. Due to the constrained coverage of the synthetic drone imagery, the textual annotations struggle to reach a semantic granularity sufficient for characterizing scene details, resulting in low retrieval accuracy.

CVG-text Dataset: Ye et al. [11] introduced a city-level CMGL dataset, employing GPT-4o [39] to generate descriptive text for 30,000 scene points across three major cities, i.e., New York, Brisbane and Tokyo. While this dataset enhances textual richness through Large Language Models, its restricted geographical span limits the model’s capability to represent complex natural landscapes. Furthermore, CVGText focuses primarily on modern metropolitan environments and generic semantics, leading to insufficient characterization of intrinsic physical attributes and hindering its adaptability to global-scale environmental heterogeneity.

GeoLoc Dataset: Recently, Song et al. [16] proposed a CMGL dataset spanning 36 global regions, which encom-

passes 52,684 multi-view image-text pairs. A notable advantage of this dataset is its support for highly flexible mutual querying between textual descriptions and multi-view imagery. However, constrained by its limited data volume and regional diversity, GeoLoc struggles to comprehensively capture the extensive spatial heterogeneity at a global scale.

Overall, existing dedicated datasets for cross-modal geolocalization remain insufficient to address localization challenges in diverse global environments. Consequently, it is imperative to establish a comprehensive and large-scale CMGL dataset integrating geographically diverse imagery and fine-grained textual descriptions.

B. Geo-localization Methods

To motivate cross-modal geo-localization on a global scale, we discuss existing CVGL methods in the remote sensing domain and potential techniques from the field of text-to-image retrieval that could be adapted for CMGL in the subsequent sections.

1) *CVGL Methods*: Cross-View Geo-localization (CVGL) has emerged as a pivotal research area. Workman et al. [17] pioneered this field by demonstrating that deep neural features offer superior generalization over traditional hand-crafted descriptors. Early research primarily focused on establishing robust feature extraction frameworks [40]–[42], while contemporary approaches emphasize architectural modernization by integrating Transformer-based global modeling and MLP-Mixer designs [4], [5], [7], [22], [43] to capture long-range spatial dependencies. Beyond feature extraction, a fundamental motivation in CVGL is to bridge the geometric and semantic discrepancies between disparate perspectives. Some methodologies strive to achieve cross-view alignment through contrastive learning and hard negative mining, thereby enhancing

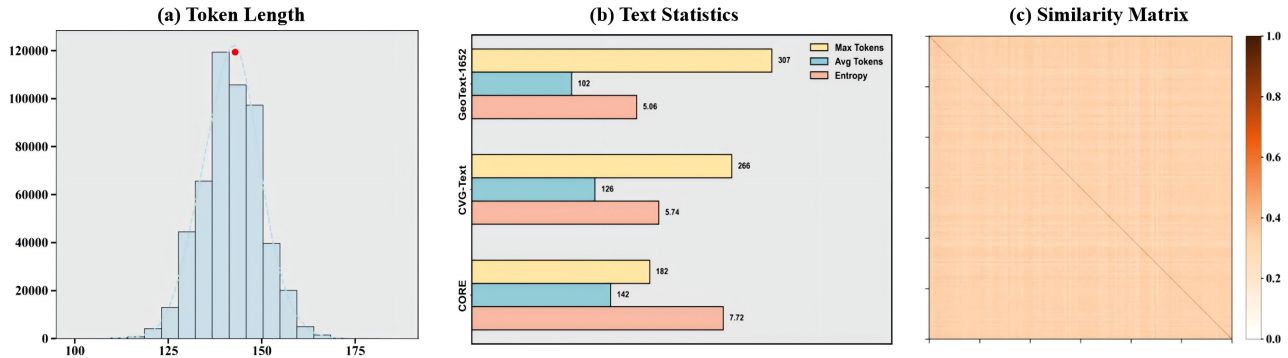


Fig. 6. Overview of text feature statistics in CORE dataset. (a) Token length distribution histogram; (b) Text statistics comparison between the CORE dataset and existing CMGL datasets; (c) Text similarity matrix.

training, preventing the network from overfitting to environmental features or architectural styles unique to a specific continent. Furthermore, such a partitioning scheme facilitates rigorous cross-continent generalization testing, enabling a comprehensive assessment of the model’s ability to adapt to heterogeneous and previously unseen global domains.

B. Data Annotation

To mitigate the cross-modal misalignment between visual scenes and natural language, we establish a structured prompting framework to generate fine-grained annotations via Qwen3-VL-Plus⁴. Fig. 4 illustrates the descriptive process for the CORE dataset. The annotation pipeline employs a progressive scene analysis strategy, systematically guiding the model to construct a comprehensive environmental profile for each sampling location. Specifically, the prompt constrains the model to observe the scene from a first-person pedestrian perspective, sequentially describing architectural typologies, road geometries, and environmental elements. This process prioritizes the extraction of intrinsic physical attributes, such as building heights, façade materials, chromatic characteristics, and vegetation density. To facilitate spatial reasoning, we further incorporate egocentric spatial cues to define the relative positions of these elements. This systematic characterization is specifically designed to align with realistic user-centric queries, ensuring that the generated descriptions are both intuitive and practical for real-world localization tasks. To ensure high consistency across samples, the generated descriptions follow a unified structural template, maintaining a synchronized narrative order from street layout to atmospheric conditions. Regarding quality control, we implement a rigorous protocol involving comprehensive manual inspection. Specifically, we extract 10% of the image-text pairs (approximately 50000) from the dataset for manual expert review, involving 10 human evaluators with domain knowledge and requiring around 300 hours of work. These pairs are distributed proportionally across all 225 geographic regions. Beyond filtering malformed responses, human evaluators manually purged entries with

hallucinated landmarks, visual-textual contradictions or illogical spatial narratives. The error patterns identified through this rigorous validation process are subsequently utilized to formulate heuristic rules for filtering the remaining unchecked data, ensuring that the final generated image-text pairs exhibit high accuracy and semantic integrity.

C. Data Analysis

Compared with existing datasets in geo-localization, the CORE dataset exhibits unique properties in geographical diversity, scale diversity, and scene diversity. Particular physical attribute mining and fine-grained information density are also defining characteristics that set CORE apart from traditional benchmarks.

1) *Data Characteristics*: The CORE dataset is distinguished by five characteristics that facilitate robust global-scale geo-localization:

- **Geographical Diversity**: CORE dataset spans 225 distinct regions across six continents, encompassing a broad spectrum from high-density urban centers to sprawling suburban landscapes. As illustrated in Fig. 3, this extensive sampling strategy is designed to mitigate overfitting to specific architectural styles or regional surface textures. By introducing high geographical heterogeneity, the dataset encourages models to learn robust, domain-agnostic feature representations.
- **Scale Diversity**: By integrating multi-source street-level and high-resolution satellite imagery, CORE establishes a hierarchical framework supporting localization at city, continental, and global scales. This multi-scale architecture facilitates fine-grained street-texture matching while enabling cross-regional validation across vast territories. Such a design provides a comprehensive benchmark for evaluating the spatial robustness of localization algorithms at varying granularities.
- **Scene Diversity**: To ensure global localization consistency, CORE incorporates a highly heterogeneous scene distribution. As illustrated in Fig. 3, the global sampling spans multiple continents, achieving multi-dimensional coverage from dense urban centers to expansive suburban

⁴<https://github.com/QwenLM/Qwen3-VL>

areas. This geographic breadth is highly consistent with the fine-grained vocabulary shown in Fig. 5, characterizing both structured urban elements and suburban features such as vegetation, terrain, and road textures. Such coherent modeling, bridging macro-distribution with micro-attributes, enables the data to transcend transient visual appearances for deep semantic alignment.

- **Physical Attribute Profiling:** A defining merit of the CORE dataset lies in its emphasis on intrinsic physical signature characterization, which prioritizes immutable physical realities over transient phenomena. Annotations systematically encode geometric dimensions, material compositions, and chromatic attributes, translating visual perception into structured features. This rigorous descriptive methodology empowers models to achieve a deeper understanding of the underlying physical essence across heterogeneous geographic scenes.
- **Fine-grained Tokens:** Fig. 6(a) shows that token lengths in core primarily range from 125 to 175, peaking at 140. This Gaussian-like, fine-grained sample structure ensures semantic depth while enhancing training robustness. Serving as the query-side, these high-density tokens provide precise signals that enrich the discriminative power of the feature space. Such detailed cues strengthen cross-modal alignment in the manifold space, ensuring superior localization stability even in image-constrained scenarios.

2) *Data Statistics and Visualization:* The quantitative statistical results regarding the textual descriptions of CORE dataset are illustrated in fig. 6(b). CORE dataset significantly outperforms datasets such as Geotext-1652 and CVG-Text in both average token length and entropy, reflecting superior informational density and scene-characterization capabilities. Meanwhile, the lower maximum token count of CORE effectively circumvents attention dispersion inherent in excessively long sequences. Fig. 6(c) illustrates a text similarity matrix with minimal cross-sample correlation, verifying the high independence of the generated descriptions. This low-similarity characteristic ensures that each description uniquely and precisely represents its specific geographic scene, effectively mitigating the risk of inter-scene semantic confusion.

IV. METHOD

Formally, CMGL is formulated as a fine-grained image-text retrieval task. Given a query set of street-view descriptions \mathcal{T} and a gallery of N geo-tagged satellite images $\mathcal{S} = \{I_1, I_2, \dots, I_N\}$, the objective is to retrieve the ground-truth image spatially corresponding to a specific query $T \in \mathcal{T}$. This process is mathematically defined as identifying the target image \hat{I} that maximizes the cross-modal similarity in a shared latent space:

$$\hat{I} = \arg \max_{I_k \in \mathcal{S}} \text{sim}(\Phi_{\text{txt}}(T), \Phi_{\text{img}}(I_k)) \quad (1)$$

where $\Phi_{\text{txt}}(\cdot)$ and $\Phi_{\text{img}}(\cdot)$ denote the textual and visual encoders that extract global semantic representations, and $\text{sim}(\cdot, \cdot)$ represents the cosine similarity metric. Building upon

this general retrieval paradigm, the proposed PLANET framework introduces intrinsic physical constraints to enhance the environmental discriminability of the feature encoders.

Fig. 7 presents the overall architecture of the proposed PLANET, which is composed of three integral parts. First, considering that standard encoders struggle to capture inherent fine-grained physical attributes from pixel distributions, an intrinsic physical signature mining module is proposed. This module explicitly decouples the statistical distribution patterns of satellite imagery to mine essential physical signatures, accurately characterizing surface morphology across color, spatial structure, and texture dimensions. Second, for the main backbone, the framework adopts a general dual-stream vision-language architecture, employing a visual encoder and a textual encoder to independently extract global semantic representations from satellite imagery and street-view descriptions, respectively. To bridge the semantic gap between abstract linguistic concepts and visual reality, physical semantic projectors are introduced following the textual branch. These projectors map high-level textual features into fine-grained physical attribute descriptors, effectively translating linguistic descriptions into structured physical codes while maintaining global feature extraction. Finally, to ensure precise cross-modal interaction at the attribute level, a consistency contrastive learning paradigm is introduced. This mechanism enforces the alignment between the mined image physical signatures and the projected textual descriptors, guiding the textual branch to model geographical prior constraints. By jointly optimizing the global contrastive loss and this physical consistency constraint, the model’s environmental-discriminative power in heterogeneous global scenarios is significantly enhanced.

A. Intrinsic Physical Signature Mining

To endow the model with explicit perception of the physical environment, we design the **Intrinsic Physical Signature Mining** module. Distinct from traditional methods [52], [53], which treats handcrafted features as supplementary inputs to the network, our motivation is fundamentally different: **we utilize these statistical characteristics as supervision signals, not input features.** The key philosophy is that physical laws (e.g., spectral distribution, geometric layout) serve as objective ground truths. By mining intrinsic statistical distribution patterns from satellite imagery, we construct a set of non-parametric physical anchors designed to guide the deep network in learning a semantic space that aligns with physical reality, rather than merely unexplainable features. This constitutes a physical consistency mechanism. Specifically, by explicitly decoupling the statistical distribution patterns of the images, we extract physically interpretable signatures along three orthogonal dimensions: spectral chromaticity, geometric Structure, and surface Texture.

1) *Spectral Chromaticity Mining:* Spectral distribution serves as the most intuitive physical attribute for distinguishing land cover types (e.g., vegetation, water bodies, man-made structures). To capture macro-level spectral priors that reflect the statistical expectation of material composition, we utilize

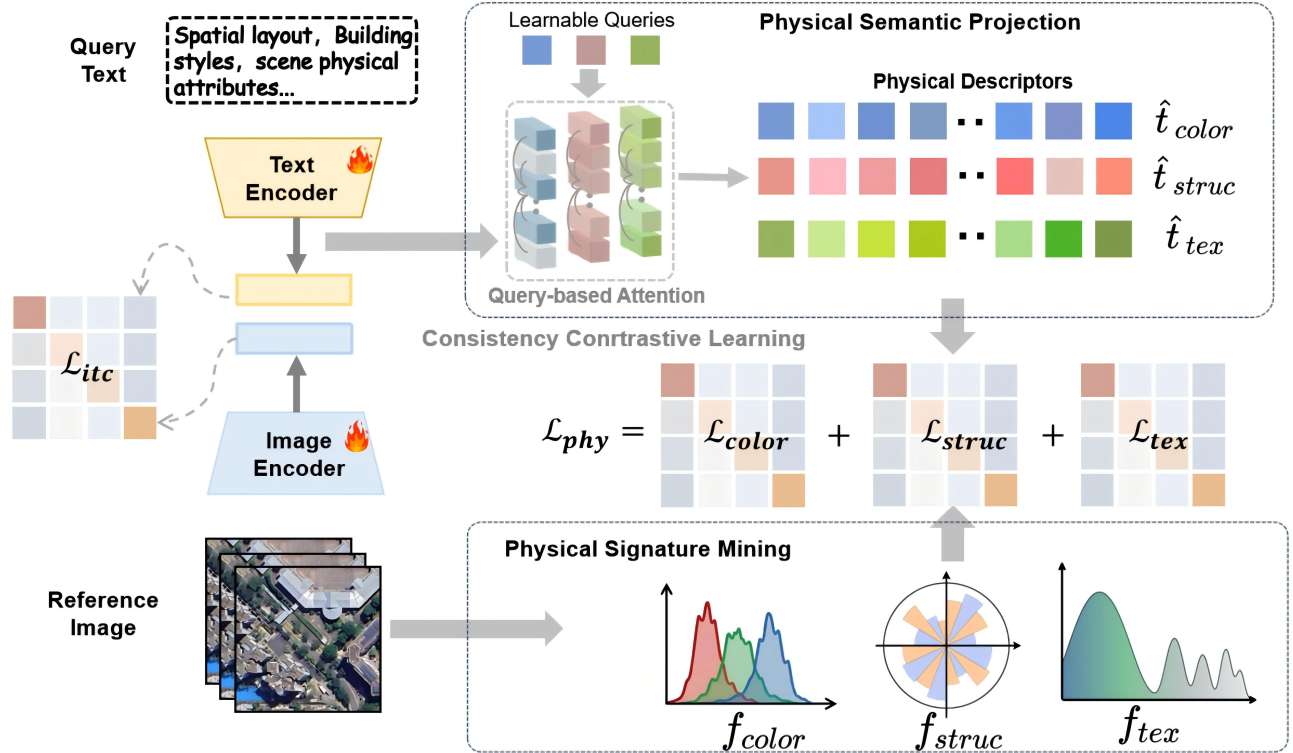


Fig. 7. Pipeline of proposed PLANET. The model consists of vision-language foundation architecture, physical signature mining module and physical semantic projection module. In the visual branch, the physical signature mining module extracts deterministic, domain-invariant physical anchors. Concurrently, the textual branch performs physical semantic projection via learnable queries, explicitly deconstructing linguistic sequence features into attribute-specific descriptors. The framework is jointly optimized through holistic semantic alignment and a fine-grained physical consistency loss.

statistical color histograms [54] as supervision targets. Given an input image I , each color channel is quantized into fixed discrete bins. The normalized frequency $h_{color}^c(k)$ for the k -th bin of channel c is calculated as:

$$h_{color}^c(k) = \frac{1}{HW} \sum_{x,y} \mathbb{I}(I_c(x,y) \in bin_k) \quad (2)$$

where $\mathbb{I}(\cdot)$ is the indicator function. The concatenation of histograms from all channels constitutes the spectral chromaticity signature f_{color} , providing prior constraints regarding material composition.

2) *Geometric Structure Mining*: Geometric structure reflects the macroscopic spatial layout and orientation of major scene elements (e.g., road extensions, building alignments). To capture this macroscopic structural information and guide the model to focus on dominant orientations, we leverage the histogram of gradient orientations [55]. First, we compute the gradient magnitude $M(x,y)$ and orientation $\theta(x,y) \in [0, \pi]$. To mitigate background noise interference and focus on salient structures, an adaptive masking mechanism is introduced. This mechanism filters out low-frequency flat regions via gradient-based relative thresholding, defining the valid structure set Ω :

$$\Omega = \{(x,y) \mid M(x,y) > \tau_{rel} \cdot \max_{i,j} M(i,j)\} \quad (3)$$

where τ_{rel} denotes the suppression coefficient and is set to 0.15. Subsequently, we construct the geometric structure

signature f_{struc} by computing the histogram of normalized orientations within Ω . This feature effectively encodes the dominant directionality of the scene, remaining invariant to specific spatial translations.

3) *Surface Texture Mining*: Surface texture describes the roughness and microscopic complexity of surface materials. To characterize these high-frequency details, we employ the histogram of laplacian energy distribution [56]. First, the second-order Laplacian operator ∇^2 is applied to extract the high-frequency response energy $E(x,y) = |\nabla^2 I(x,y)|$. Given that the texture energy of natural scenes typically exhibits a heavy-tailed distribution, direct histogramming would result in excessive clustering in low-energy regions. Therefore, a logarithmic transformation is applied to rectify the distributional skewness, enhancing the separability of high-energy texture details:

$$E_{log}(x,y) = \log(1 + E(x,y)) \quad (4)$$

Next, we map the energy to the $[0,1]$ interval via dynamic maximum normalization and compute its distribution histogram as the surface texture signature f_{tex} . This signature effectively distinguishes diverse surface material properties by capturing the statistical shape of the energy distribution, thereby enabling the explicit differentiation between sparse strong edges and dense weak textures.

Ultimately, by concatenating these three physical components, we construct the comprehensive intrinsic physical signa-

ture $P_{sig} = [f_{color} || f_{struc} || f_{tex}]$, providing a robust physical supervision anchor for cross-modal alignment.

B. Multi-modal Feature Encoding and Physical Semantic Projection

To establish a robust correspondence between ground-level descriptions and satellite imagery, our PLANET framework operates on a dual-stream architecture that harmonizes high-level global semantics with fine-grained physical laws.

1) *Global Dual-Stream Encoding & Contrastive Alignment:* We employ a dual-stream backbone consisting of an image encoder Φ_{img} and a text encoder Φ_{txt} to extract representations from the satellite image I and the description T .

In the visual branch, the image encoder Φ_{img} maps the satellite image into a normalized global embedding vector $v \in \mathbb{R}^D$, which encapsulates the holistic scene context. In the textual branch, for the transformer-based text encoder Φ_{txt} , we extract features at two distinct levels. First, we obtain a global semantic embedding $t \in \mathbb{R}^D$ representing the macro-meaning of the entire description, which is acquired by extracting the final aggregated features of the text sequence.

To ensure global semantic consistency between modalities, we apply the standard InfoNCE loss [57] on these global features. For a batch of N image-text pairs, the global alignment objective \mathcal{L}_{itc} is formulated as:

$$\mathcal{L}_{itc} = -\frac{1}{N} \sum_{i=1}^N \log \frac{\exp(\text{sim}(v_i, t_i)/\tau)}{\sum_{j=1}^N \exp(\text{sim}(v_i, t_j)/\tau)} \quad (5)$$

where $\text{sim}(\cdot, \cdot)$ denotes cosine similarity and τ is a learnable temperature parameter. While \mathcal{L}_{itc} aligns the general semantic space, it often fails to capture specific physical attributes, such as color distribution or geometric structural orientation, due to the heavy information compression in a single global vector [58].

2) Physical Semantic Projection via Learnable Queries:

To explicitly disentangle intrinsic physical properties from the linguistic stream, we introduce a dedicated physical semantic projection module. Unlike standard linear projections that operate on global tokens, our projection mechanism leverages the full sequence of token embeddings $E_{txt} \in \mathbb{R}^{L \times D}$ from the last hidden layer of the text encoder, where L is the sequence length. This sequence preserves fine-grained semantic details and attribute cues for each word, avoiding information loss.

Inspired by the success of querying mechanisms in recent large vision-language models [46], we implement the projection heads using a set of learnable physical queries, denoted as $Q_{color}, Q_{struc}, Q_{tex} \in \mathbb{R}^D$. These queries act as semantic anchors for the projection, optimized end-to-end to dynamically aggregate attribute-specific information from the sequence E_{txt} . Following the standard scaled dot-product attention mechanism [59], for each physical dimension $k \in \{color, struc, tex\}$, the projected physical descriptors \hat{t}_k are computed as:

$$A_k = \text{Softmax} \left(\frac{Q_k (E_{txt} W_K)^T}{\sqrt{D}} \right), \quad (6)$$

$$\hat{t}_k = \text{LayerNorm} (A_k (E_{txt} W_V))$$

where $A_k \in \mathbb{R}^{1 \times L}$ serves as the projection attention map, highlighting tokens relevant to the specific physical attribute. For instance, the color query vector automatically attends to color-descriptive terms, while the transformation matrices W_K and W_V handle the feature space mapping. Instead of compressing the sentence into a highly entangled global representation, this query-driven attention mechanism explicitly deconstructs the holistic semantics into a fine-grained form that is dynamically queryable by distinct physical attributes. Consequently, this design ensures that the projected descriptors \hat{t}_k are strictly aligned with the visual physical signatures, facilitating subsequent physical consistency learning.

C. Consistency Contrastive Learning

Following the physical semantic projection, the core challenge of PLANET is to ensure that the projected descriptors \hat{t}_k align with the ground-truth physical reality. To this end, we propose a **Consistency Contrastive Learning** paradigm that utilizes the intrinsic physical signatures mined from satellite imagery as direct supervision signals.

1) *Intrinsic Physical Supervision:* As described in Sec. IV-A, we harvest three orthogonal physical signatures from the satellite imagery: spectral chromaticity f_{color} , geometric structure f_{struc} , and surface texture f_{tex} . Since our physical semantic projectors (Sec. IV-B) are explicitly designed to map textual representations into the same metric space as these statistical distributions, we treat $f_{color}, f_{struc}, f_{tex}$ directly as the unlearnable ground truth anchors for their respective physical dimensions.

2) *Fine-grained Consistency Objective:* To achieve precise geo-localization, the model must explicitly align the textually projected physical semantics with the deterministic visual statistics of the image. For instance, the color descriptors projected by the color query should statistically match the image’s color signature. We formulate this via a physical consistency loss \mathcal{L}_{phy} . For a batch of N samples, we compute the contrastive loss across the three physical dimensions:

$$\mathcal{L}_{phy} = \sum_k -\frac{1}{N} \sum_{i=1}^N \log \frac{\exp(\text{sim}(\hat{t}_{k,i}, f_{k,i})/\tau_p)}{\sum_{j=1}^N \exp(\text{sim}(\hat{t}_{k,i}, f_{k,j})/\tau_p)} \quad (7)$$

where $\hat{t}_{k,i}$ is the projected physical descriptor, $f_{k,i}$ is the mined physical signature of the corresponding image, and τ_p is a dedicated temperature parameter. Unlike the global alignment objective, \mathcal{L}_{phy} forces the text encoder to learn interpretably, ensuring that specific linguistic cues (e.g., “red roofs”, “grid layout”) are correctly mapped to their corresponding physical manifestations without semantic drift.

3) *Joint Optimization Objective:* The PLANET framework is optimized in an end-to-end manner. The total loss function \mathcal{L}_{total} fuses the holistic semantic alignment with the fine-grained physical consistency:

$$\mathcal{L}_{total} = \mathcal{L}_{itc} + \lambda \mathcal{L}_{phy} \quad (8)$$

where λ is the sole hyper-parameter balancing global semantic understanding and physical grounding. We deliberately

TABLE II
 QUANTITATIVE RESULTS OF PLANET AND EXISTING METHODS ON CORE DATASET. WE REPORT THE RETRIEVAL RECALL ($R@1$) AND LOCALIZATION ACCURACY ($L@150$) ACROSS THE WORLD-LEVEL AND FOUR INTERCONTINENTAL SUBSETS. BOLD INDICATES THE BEST RESULT, AND UNDERLINE INDICATES THE SECOND BEST RESULT.

Method	Global-level		Intercontinental-level							
	All		Subset1		Subset2		Subset3		Subset4	
	R@1	L@150	R@1	L@150	R@1	L@150	R@1	L@150	R@1	L@150
ViLT [60]	23.05	26.23	24.43	23.18	22.08	25.34	25.58	30.79	19.65	25.07
X-VLM [50]	26.97	30.81	28.90	30.65	25.72	28.74	28.67	33.86	24.31	29.62
X2-VLM [51]	34.35	38.33	35.79	38.5	33.73	36.56	36.12	41.25	31.43	36.61
SigLIP-B/16 [48]	30.10	34.08	29.13	31.87	30.87	33.92	31.23	36.18	28.98	34.20
SigLIP-SO400M [48]	43.27	47.48	45.03	47.74	48.26	51.34	40.71	46.15	39.14	44.69
EVA2-CLIP-B/16 [48]	41.02	44.17	42.18	44.74	43.77	46.96	37.32	42.37	37.39	42.73
EVA2-CLIP-L/14 [48]	45.38	49.56	47.59	50.40	49.44	52.52	41.03	46.31	43.98	49.41
CLIP-B/16 [24]	40.11	44.16	42.18	44.74	43.77	46.96	37.32	42.37	37.39	42.73
CLIP-L/14 [24]	44.63	48.92	45.75	48.42	49.19	53.14	41.48	46.56	42.53	47.76
BLIP [25]	42.85	46.73	45.59	48.40	48.38	51.34	39.77	44.66	37.93	42.73
RemoteCLIP [26]	42.77	46.90	44.79	47.66	47.51	50.45	40.55	45.78	38.26	43.67
TAG-CLIP [32]	38.46	42.47	38.15	40.78	42.35	45.32	37.32	42.37	36.46	41.73
Long-CLIP [27]	51.34	55.46	52.78	55.34	<u>59.85</u>	<u>62.93</u>	45.40	50.50	47.96	53.59
CrossText2Loc [11]	<u>51.92</u>	<u>55.88</u>	<u>53.12</u>	<u>55.88</u>	<u>59.36</u>	<u>62.37</u>	<u>46.97</u>	<u>51.27</u>	<u>48.71</u>	<u>54.61</u>
PLANET (Ours)	55.84	59.66	57.90	60.72	64.74	67.58	49.81	54.13	51.35	56.65

exclude specific weights for individual physical branches, positing that color, structure, and texture constitute orthogonal and equally indispensable components of the physical environment. This egalitarian design simplifies the optimization landscape and prevents the model from overfitting to any single dominant physical attribute.

V. EXPERIMENTS AND ANALYSIS

A. Benchmark

We establish a benchmark on the CORE dataset for CMGL tasks across two distinct scales: **World-level** and **Intercontinental-level**. The World-level benchmark validates the model’s global-scale retrieval capability on the complete dataset, while the Intercontinental-level benchmark evaluates both the domain-specific performance within the four geographical partitions (Sec.III) and its out-of-distribution generalization via a cross-regional evaluation paradigm. To provide a comprehensive assessment, we adopt retrieval accuracy and localization precision as the two primary evaluation dimensions. For the retrieval dimension, following standard protocols in cross-view geo-localization [17], we employ $R@1$ as the principal metric, measuring the percentage of query images correctly matched to their ground-truth satellite imagery. For the localization dimension, given the unprecedented geographic breadth and high spatial discreteness of the CORE dataset, we diverge from the conventional $L@50$ standard [12], [61] and instead establish $L@150$ as the primary metric. This denotes the proportion of queries where the geodesic distance between the predicted result and the actual location is less than 150 meters.

B. Implementation Details

Regarding data partitioning, we strictly divide each geographical subset of the CORE dataset into training and testing sets at a 9:1 ratio. We employ the OpenAI pre-trained CLIP-ViT-L/14@336px [24] model as the backbone for both visual and textual encoders. Consistent with standard evaluation protocols [11], the input resolution of satellite imagery is resized to 336×336 . Furthermore, the embedding sequence length of text context is extended to 300 tokens to fully accommodate the fine-grained physical descriptions within the CORE dataset. All experiments are implemented using the PyTorch framework on two NVIDIA GeForce RTX 4090 GPUs and 48GB memory. The models are trained for 40 epochs with a batch size of 32. We utilize the Adam [62] optimizer with an initial learning rate of 1×10^{-5} , which is decayed via a cosine annealing schedule.

C. Results and Analysis

Comparison With Baselines: To evaluate the effectiveness of the proposed PLANET framework and provide guidance for future large-scale CMGL task led by CORE, we conduct a comprehensive evaluation and analyze the results of 14 cross-modal retrieval methods [11], [24]–[28], [32], [48], [50], [51], [60]. Table II provides a comprehensive benchmark on CORE, including detailed quantitative analyses of the “World-level” and four “Intercontinental-level” subsets. The benchmark methods cover a variety of architectures, including standard vision-language models such as CLIP and SigLIP, as well as specialized spatial retrieval methods such as Cross-Text2Loc and TAG-Clip. All experiments are based on a standard training schedule. It can be seen that our PLANET significantly outperforms existing methods in all metrics and ge-

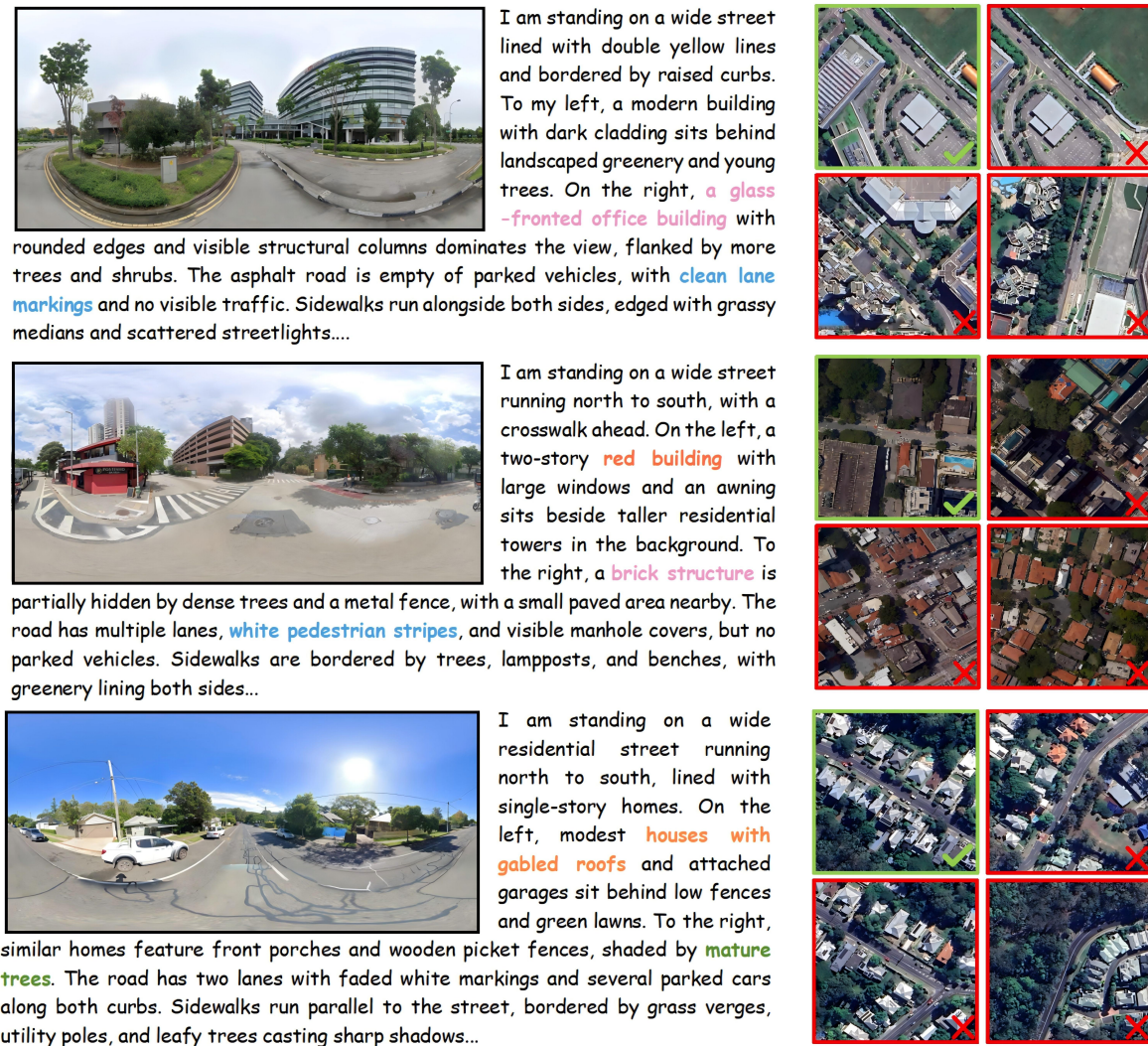


Fig. 8. The retrieval results of PLANET on CORE dataset. The left side displays the original street view image along with its corresponding textual description. The right side illustrates the top four retrieval results, where green highlights indicate correct matches and red highlights signify incorrect results.

ographic partitions. Specifically, in highly challenging global benchmarks, PLANET achieves 55.84% on R@1 and 59.66% on L@150, representing significant improvements of 3.92% and 3.78% in retrieval accuracy and localization accuracy, respectively, compared to the strong baseline CrossText2Loc. Furthermore, PLANET demonstrates consistent performance improvements across all four intercontinental-level subsets, highlighting its robustness to diverse geographic environments and architectural styles. Compared to existing methods, it maintains an average lead of approximately 2.84 - 4.89% in R@1 and 2.86 -5.38% in L@150 in these regions.

Qualitative Results and Visualization: Fig. 8 shows representative cross-modal geolocation visualizations on CORE dataset. For each query text, we present the top-4 image retrieval results, with true matches marked with green boxes. The results demonstrate that our PLANET effectively mines fine-grained physical cues, such as structure, color and texture, implicit in the query text, thereby accurately retrieving the

correct matched satellite images from the candidate lists in various complex scenarios. This fully demonstrates that PLANET can eliminate intermodal gaps, thus achieving robust cross-modal semantic alignment.

D. Ablation Studies

1) *Effectiveness of Physical Consistency Mechanism:* In the methodology phase, we establish a holistic physical consistency mechanism for PLANET, systematically integrating intrinsic physical signature mining, physical semantic projection, and consistency contrastive learning. To validate the effectiveness of this mechanism, we conduct extensive ablation studies across the four intercontinental subsets of the CORE dataset. Specifically, we incrementally introduce individual physical priors into the baseline and compare the results against the fully integrated architecture to assess their respective contributions. As illustrated in Table III, the introduction of any single physical constraint (f_{color} , f_{struc} ,



Fig. 9. Top-3 retrieval results and heatmaps on the corresponding satellite images from baseline and PLANET. The introduction of physical consistency constraints enables PLANET to more accurately anchor its attention on crucial geographical regions.

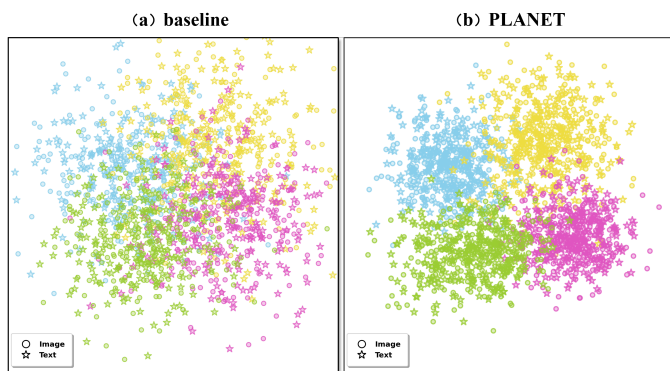


Fig. 10. UMAP visualization of the feature distribution of the CORE dataset. Compared to the baseline (left), PLANET (right) significantly enhances the discriminative power of features by introducing physical property constraints. Samples from different subsets (distinguished by color) exhibit higher intra-class cohesion and clearer inter-class boundaries in space, while achieving tighter cross-modal alignment between images (circles) and text (stars).

or f_{tex}) in the baseline consistently enhances performance across all continental subsets. This finding indicates that even single-dimensional physical cues can effectively mitigate the limitations of global semantic features in fine-grained scene differentiation. Quantitatively, individual constraints produce an average improvement in R@1 of 1.87% -2.00% over

the baseline in diverse regions. In addition, the complete PLANET model achieves superior performance, surpassing all variants with a single-attribute. Specifically, it outperforms the best single-branch variant by a further 1.40%–2.16% in R@1. This outcome confirms that spectral color, geometry, and surface texture represent orthogonal information sources, thereby constructing a comprehensive physical representation independent of high-level semantics.

To intuitively validate the efficacy of our physical consistency mechanism, we visually compare the heatmaps generated by PLANET and the baseline on the corresponding satellite image. As shown in Fig.9, heatmap from the baseline is diffuse and unfocused, struggling to isolate specific attributes from the broader scene context, which leads to incorrect retrieval results. In contrast, PLANET demonstrates superior physical grounding capability, accurately activating local regions by perceiving key physical attribute terms such as “red-tiled roofs”, “tall, leafy trees” and “white edge lines” effectively decoupling different physical attributes that are confused by the baseline model.

2) *Ablation on Weighting Coefficients of Physical Constraints*: In the implementation of PLANET, we uniformly set the weighting coefficients for the three physical consistency constraints to $\frac{1}{3}$. The theoretical rationale for this setting is twofold. First, assigning equal weights ensures fairness among

TABLE III
 ABLATION STUDY ON PHYSICAL CONSISTENCY MECHANISM. WE INVESTIGATE THE IMPACT OF EXPLICIT PHYSICAL CONSTRAINTS BY COMPARING OUR PLANET VARIANTS AGAINST THE BASELINE .

Method	Subset 1		Subset 2		Subset 3		Subset 4	
	R@1	L@150	R@1	L@150	R@1	L@150	R@1	L@150
Baseline (w/o Physical)	53.12	55.88	59.36	62.37	46.97	51.27	48.71	54.61
+ Color (f_{color})	55.81	58.23	62.58	65.10	47.93	52.20	49.83	55.07
+ Structure (f_{struc})	55.78	58.16	62.32	64.98	48.03	52.24	49.52	55.12
+ Texture (f_{tex})	55.43	58.10	62.46	65.08	48.21	52.53	49.95	55.48
PLANET (Full)	57.90	60.72	64.74	67.58	49.81	54.13	51.35	56.65

TABLE IV

ABLATION STUDY ON THE WEIGHTING COEFFICIENTS OF THE PHYSICAL CONSISTENCY CONSTRAINTS ACROSS FOUR SUBSETS OF THE CORE DATASET. WE REPORT THE R@1 (%) METRIC. GROUP (A) VARIES THE OVERALL WEIGHT WHILE KEEPING INTERNAL RATIOS EQUAL. GROUP (B) ALTERS THE INTERNAL PROPORTIONS WHILE MAINTAINING THE OPTIMAL TOTAL WEIGHT.

Variant	Weights			\sum	R@1 (%) on CORE Subsets			
	λ_c	λ_s	λ_t		Sub 1	Sub 2	Sub 3	Sub 4
<i>(a) Ablation on Overall Weight (Fixed 1:1:1 Ratio)</i>								
Under-regularized	0.1	0.1	0.1	0.3	54.12	60.83	47.58	49.97
Under-regularized	0.2	0.2	0.2	0.6	56.43	63.15	48.76	50.66
Over-regularized	0.5	0.5	0.5	1.5	57.07	63.88	49.26	50.92
Over-regularized	1.0	1.0	1.0	3.0	54.82	60.75	48.04	50.23
<i>(b) Ablation on Internal Proportions (Fixed $\sum = 1.0$)</i>								
Biased (Color)	0.6	0.2	0.2	1.0	57.22	63.85	49.36	51.02
Biased (Struc)	0.2	0.6	0.2	1.0	57.08	63.69	49.42	50.88
Biased (Tex)	0.2	0.2	0.6	1.0	56.87	63.74	49.49	51.20
PLANET (Ours)	1/3	1/3	1/3	1.0	57.90	64.74	49.81	51.35

the three orthogonal physical dimensions during the learning process. Second, the scaling factor of $\frac{1}{3}$ maintains a balance between the aggregated expected physical loss and the cross-modal contrastive loss. To validate the effectiveness of this design, we conduct two sets of ablation studies focusing on the overall weight of the consistency contrastive learning and the internal proportions of the three variables, respectively.

First, we evaluate the impact of the overall physical consistency weight by varying the total sum from 0.3 to 3.0 while keeping the internal ratio fixed at 1:1:1. The results in Table IV show that setting the total weight to 1.0 achieves the highest retrieval accuracy across all subsets. This confirms that this scaling factor best balances the physical consistency loss with the cross-modal contrastive loss.

Second, with the total weight fixed at 1.0, we test different internal ratio allocations for the three physical dimensions: color, structure, and texture. As shown in Table IV, an equally distributed weight configuration consistently outperformed any bias setting favoring a single attribute, strongly validating our theoretical assumption. These three physical attributes are orthogonal and equally important; ensuring learning fairness among them during training allows for the extraction of the feature representation with the best global generalization ability.

E. Cross-Subset Generalization Experiments

The heterogeneous nature of CORE dataset, characterized by architectural styles and natural environments, inherently

TABLE V
 QUANTITATIVE COMPARISON OF OUT-OF-DISTRIBUTION GENERALIZATION ON CORE DATASET.

Method	Subset1 \rightarrow 4		Subset2 \rightarrow 4		Subset3 \rightarrow 4	
	R@1	L@150	R@1	L@150	R@1	L@150
TAG-CLIP	12.22	14.13	11.83	13.79	14.79	17.06
BLIP	15.24	17.93	14.17	16.58	16.84	19.35
CLIP-L/14	15.58	18.25	14.34	16.62	17.22	19.83
Long-CLIP	21.68	25.07	19.75	22.86	22.96	26.10
CrossText2Loc	<u>23.13</u>	<u>26.97</u>	<u>21.06</u>	<u>24.64</u>	<u>24.75</u>	<u>28.12</u>
PLANET (Ours)	28.32	32.54	26.80	30.88	30.96	35.01

TABLE VI

QUANTITATIVE COMPARISON OF DIFFERENT METHODS ON CVG-TEXT DATASET.

Method	New York		Brisbane		Tokyo	
	R@1	L@50	R@1	L@50	R@1	L@50
ViLT [60]	11.58	15.58	11.10	14.50	10.83	15.50
X-VLM [50]	15.74	16.86	15.67	17.60	12.46	14.34
X2-VLM [51]	23.33	25.17	21.58	23.67	17.83	20.75
SigLIP-B/16 [48]	19.67	21.08	19.58	22.00	15.58	17.92
SigLIP-SO400M [48]	33.50	34.83	34.25	36.83	28.42	31.50
EVA2-CLIP-B/16 [28]	25.17	26.58	28.42	31.75	22.50	25.25
EVA2-CLIP-L/14 [28]	34.08	35.67	35.67	38.00	31.00	34.08
CLIP-B/16 [24]	26.67	28.17	29.92	32.58	24.00	27.25
CLIP-L/14 [24]	35.08	37.08	34.08	37.25	28.08	30.50
BLIP [25]	34.58	37.25	34.50	38.17	29.75	33.67
RemoteCLIP [26]	33.83	36.33	32.92	34.75	26.42	29.08
TAG-CLIP [32]	31.17	33.25	29.83	31.75	24.33	28.08
Long-CLIP [27]	46.42	48.25	46.75	48.17	33.83	35.50
CrossText2Loc [11]	<u>50.33</u>	<u>53.07</u>	<u>47.58</u>	<u>51.80</u>	<u>41.75</u>	<u>43.86</u>
PLANET (Ours)	52.83	55.57	49.83	53.67	43.42	46.42

introduces significant domain shifts. To visualize how models handle this diversity under standard supervision, we project the feature embeddings of a model trained on the full dataset using UMAP technique [63]. As illustrated in fig.10, PLANET exhibits significantly tighter intra-class compactness and superior cross-modal alignment compared to baseline, where image and text features are densely coupled. While this highly discriminative latent structure correlates with our superior localization accuracy on the standard test set, it raises a critical question: Does this tight coupling stem from learning robust, domain-invariant physical laws, or merely from overfitting to domain-specific statistics?

To rigorously decouple these factors and evaluate the model’s adaptability to unseen geographic environments, we conduct cross-domain generalization experiments using Subset 4 as the target test domain. This selection is motivated by

the fact that the African and South American regions represented in Subset 4 diverge significantly from the modern urban landscapes dominant in other training subsets. They are characterized by unique physical attributes, such as unpaved road networks, specific vegetation patterns, and informal architectural styles. These distinctions constitute a substantial distribution shift, posing a severe challenge to the model’s ability to extract domain-invariant features. Specifically, we trained the model on Subsets 1–3 and subsequently validated it on the test set of Subset 4.

Table V presents the quantitative results of the cross-domain generalization experiments. Due to the distinct natural landscapes and architectural styles of the target domain compared to the training domains, all baseline models suffer severe performance degradation in the unseen environment, underscoring the formidable challenge posed by domain shifts. However, across all cross-domain settings, PLANET exhibits exceptional robustness, comprehensively and significantly outperforming the state-of-the-art methods. Specifically, in tasks where PLANET migrates from Subset 1, 2, and 3 to Subset 4, its R@1 achieves absolute performance improvements of 5.19%, 5.74%, and 6.21%, respectively, fully demonstrating its outstanding robustness in capturing domain-independent physical laws. This result validates our earlier hypothesis: the highly compact latent space learned by PLANET stems not from overfitting to domain-specific statistics, but from its successful capture of globally applicable, domain-invariant physical laws. Driven by explicit physical consistency constraints, the proposed model effectively resists drastic geographic variations, enabling accurate and stable cross-modal localization in highly heterogeneous global scenarios.

F. Results on Existing Dataset

To further validate the generalization ability and robustness of our proposed PLANET, as well as to evaluate its city-level localization performance, we conduct comparative experiments using the widely recognized CVG-Text dataset [11]. This dataset emphasizes typical modern urban environments, providing a rigorous testing platform to assess whether models can consistently establish fine-grained cross-modal physical alignments within complex, high-density urban layout.

The quantitative results shown in Table VI indicate that PLANET achieves state-of-the-art performance across all three cities, significantly surpassing existing large vision-language models and specialized geo-localization networks. Specifically, in comparison to the strongest baseline, CrossText2Loc, PLANET demonstrates absolute improvements in the R@1 metric of 2.50%, 2.25%, and 1.67% for New York, Brisbane, and Tokyo, respectively, along with consistent gains in the L@50 metric. These findings provide compelling evidence that our proposed physical consistency mechanism not only excels in highly heterogeneous global landscapes but also maintains superior feature discriminability in conventional urban scenarios.

G. Limitation

Although our PLANET framework demonstrates exceptional performance and stability in global CMGL, it is still

subject to an inherent limitation: the challenge of achieving absolute temporal synchronization between street-view and satellite imagery acquisition. Transient visual elements, such as vehicles and construction sites, introduce unavoidable noise into the cross-modal alignment process. While our intrinsic physical signature mining alleviates this issue to some extent, achieving robust localization in extreme scenarios—such as conflict zones or natural disasters—remains highly challenging. Future research will focus on data acquisition under extreme conditions and time-invariant feature mining to promote feature alignment across different modalities and further improve generalization.

VI. CONCLUSION

In this paper, we propose CORE, the first million-scale dataset dedicated to global-scale cross-modal geo-localization (CMGL). This dataset comprises 1,034,786 multi-view images captured from both ground and aerial perspectives across 225 distinct geographic regions, accompanied by textual descriptions for each ground image. The CORE dataset is highly valuable due to its substantial sample size, fine textual granularity, and pronounced geographic heterogeneity. It is anticipated to facilitate a new, challenging, yet significant task: global-scale geo-localization. Furthermore, we present PLANET, a physical-law-aware consistency contrastive learning paradigm that explicitly aligns intrinsic physical signatures—including spectral color, geometric structure, and surface texture—between imagery and text. Utilizing the CORE dataset, we establish a benchmark and empirically validate the effectiveness and generalization capability of the proposed PLANET. In future work, we aim to further enhance the scene diversity of the CORE dataset and investigate the generalizability of physical-law-aware mechanisms across a wider array of vision-language understanding tasks.

REFERENCES

- [1] H. Tian, J. Meng, W.-S. Zheng, Y.-M. Li, J. Yan, and Y. Zhang, “Loc4plan: Locating before planning for outdoor vision and language navigation,” in *Proceedings of the 32nd ACM International Conference on Multimedia*, 2024, pp. 4073–4081.
- [2] P.-E. Sarlin, C. Cadena, R. Siegwart, and M. Dymczyk, “From coarse to fine: Robust hierarchical localization at large scale,” in *Proceedings of the IEEE/CVF conference on computer vision and pattern recognition*, 2019, pp. 12 716–12 725.
- [3] F. Deuser, K. Habel, and N. Oswald, “Sample4geo: Hard negative sampling for cross-view geo-localisation,” in *Proceedings of the IEEE/CVF International Conference on Computer Vision (ICCV)*, October 2023, pp. 16 847–16 856.
- [4] P. Xia, Y. Wan, Z. Zheng, Y. Zhang, and J. Deng, “Enhancing cross-view geo-localization with domain alignment and scene consistency,” *IEEE Transactions on Circuits and Systems for Video Technology*, 2024.
- [5] Q. Wu, Y. Wan, Z. Zheng, Y. Zhang, G. Wang, and Z. Zhao, “Camp: A cross-view geo-localization method using contrastive attributes mining and position-aware partitioning,” *IEEE Transactions on Geoscience and Remote Sensing*, 2024.
- [6] X. Zhang, X. Li, W. Sultani, Y. Zhou, and S. Wshah, “Cross-view geo-localization via learning disentangled geometric layout correspondence,” in *Proceedings of the AAAI conference on artificial intelligence*, vol. 37, no. 3, 2023, pp. 3480–3488.
- [7] S. Zhu, M. Shah, and C. Chen, “Transgeo: Transformer is all you need for cross-view image geo-localization,” in *Proceedings of the IEEE/CVF Conference on Computer Vision and Pattern Recognition*, 2022, pp. 1162–1171.

- [8] Q. Zhang and Y. Zhu, "Benchmarking the robustness of cross-view geo-localization models," in *European Conference on Computer Vision*. Springer, 2024, pp. 36–53.
- [9] X. Zhang, X. Li, W. Sultani, C. Chen, and S. Wshah, "Geodtr+: Toward generic cross-view geolocalization via geometric disentanglement," *IEEE Transactions on Pattern Analysis and Machine Intelligence*, vol. 46, no. 12, pp. 10419–10433, 2024.
- [10] M. Chu, Z. Zheng, W. Ji, T. Wang, and T.-S. Chua, "Towards natural language-guided drones: Geotext-1652 benchmark with spatial relation matching," in *European Conference on Computer Vision*. Springer, 2024, pp. 213–231.
- [11] J. Ye, H. Lin, L. Ou, D. Chen, Z. Wang, Q. Zhu, C. He, and W. Li, "Where am i? cross-view geo-localization with natural language descriptions," in *Proceedings of the IEEE/CVF International Conference on Computer Vision*, 2025, pp. 5890–5900.
- [12] M. Kolmet, Q. Zhou, A. Ošep, and L. Leal-Taixé, "Text2pos: Text-to-point-cloud cross-modal localization," in *Proceedings of the IEEE/CVF conference on computer vision and pattern recognition*, 2022, pp. 6687–6696.
- [13] J. Chen, D. Barath, I. Armeni, M. Pollefeys, and H. Blum, "“where am i?” scene retrieval with language," in *European Conference on Computer Vision*. Springer, 2024, pp. 201–220.
- [14] D. M. Theobald, D. Harrison-Atlas, W. B. Monahan, and C. M. Albano, "Ecologically-relevant maps of landforms and physiographic diversity for climate adaptation planning," *PLoS one*, vol. 10, no. 12, p. e0143619, 2015.
- [15] A. Sağ̃söz, Ö. İ. Tuluk, and S. Özgen, "Influences of different ages and cultures on each other from architectural point of view: Examination of historical buildings in trabzon/turkiye," *Building and environment*, vol. 41, no. 1, pp. 45–59, 2006.
- [16] Z. Song, J. Zhang, D. Wang, Z. Zhou, W. Liu, H. Guo, E. Wang, and B. Du, "Geobridge: A semantic-anchored multi-view foundation model bridging images and text for geo-localization," *arXiv preprint arXiv:2512.02697*, 2025.
- [17] S. Workman, R. Souvenir, and N. Jacobs, "Wide-area image geolocalization with aerial reference imagery," in *Proceedings of the IEEE International Conference on Computer Vision*, 2015, pp. 3961–3969.
- [18] L. Liu and H. Li, "Lending orientation to neural networks for cross-view geo-localization," in *Proceedings of the IEEE/CVF conference on computer vision and pattern recognition*, 2019, pp. 5624–5633.
- [19] S. Zhu, T. Yang, and C. Chen, "Vigor: Cross-view image geo-localization beyond one-to-one retrieval," in *Proceedings of the IEEE/CVF Conference on Computer Vision and Pattern Recognition*, 2021, pp. 3640–3649.
- [20] Z. Zheng, Y. Wei, and Y. Yang, "University-1652: A multi-view multi-source benchmark for drone-based geo-localization," in *Proceedings of the 28th ACM international conference on Multimedia*, 2020, pp. 1395–1403.
- [21] J. Ye, Z. Lv, W. Li, J. Yu, H. Yang, H. Zhong, and C. He, "Cross-view image geo-localization with panorama-bev co-retrieval network," in *European Conference on Computer Vision*. Springer, 2024, pp. 74–90.
- [22] G. Huang, Y. Zhou, L. Zhao, and W. Gan, "Cv-cities: Advancing cross-view geo-localization in global cities," *IEEE Journal of Selected Topics in Applied Earth Observations and Remote Sensing*, 2024.
- [23] P. Xia, L. Yu, Y. Wan, Q. Wu, P. Chen, L. Zhong, Y. Yao, D. Wei, X. Liu, L. Ru *et al.*, "Cross-view geo-localization with panoramic street-view and vhr satellite imagery in decentrality settings," *ISPRS Journal of Photogrammetry and Remote Sensing*, vol. 227, pp. 1–11, 2025.
- [24] A. Radford, J. W. Kim, C. Hallacy, A. Ramesh, G. Goh, S. Agarwal, G. Sastry, A. Askell, P. Mishkin, J. Clark *et al.*, "Learning transferable visual models from natural language supervision," in *International conference on machine learning*. PMLR, 2021, pp. 8748–8763.
- [25] J. Li, D. Li, C. Xiong, and S. Hoi, "Blip: Bootstrapping language-image pre-training for unified vision-language understanding and generation," in *International conference on machine learning*. PMLR, 2022, pp. 12888–12900.
- [26] F. Liu, D. Chen, Z. Guan, X. Zhou, J. Zhu, Q. Ye, L. Fu, and J. Zhou, "Remotclip: A vision language foundation model for remote sensing," *IEEE Transactions on Geoscience and Remote Sensing*, vol. 62, pp. 1–16, 2024.
- [27] B. Zhang, P. Zhang, X. Dong, Y. Zang, and J. Wang, "Long-clip: Unlocking the long-text capability of clip," in *European conference on computer vision*. Springer, 2024, pp. 310–325.
- [28] Y. Fang, Q. Sun, X. Wang, T. Huang, X. Wang, and Y. Cao, "Eva-02: A visual representation for neon genesis," *Image and Vision Computing*, vol. 149, p. 105171, 2024.
- [29] T. Chen, S. Kornblith, M. Norouzi, and G. Hinton, "A simple framework for contrastive learning of visual representations," in *International conference on machine learning*. PMLR, 2020, pp. 1597–1607.
- [30] C. Wei, H. Fan, S. Xie, C.-Y. Wu, A. Yuille, and C. Feichtenhofer, "Masked feature prediction for self-supervised visual pre-training," in *Proceedings of the IEEE/CVF conference on computer vision and pattern recognition*, 2022, pp. 14668–14678.
- [31] H. Wang, X. Wu, Z. Huang, and E. P. Xing, "High-frequency component helps explain the generalization of convolutional neural networks," in *Proceedings of the IEEE/CVF Conference on Computer Vision and Pattern Recognition (CVPR)*, June 2020.
- [32] X. Zhou, Y. Wu, J. Ma, W. Wang, M. Cao, and M. Ye, "Text-based aerial-ground person retrieval," *arXiv e-prints*, pp. arXiv–2511, 2025.
- [33] M. Alizadeh, M. Kubli, Z. Samei, S. Dehghani, J. D. Bermeo, M. Korobeynikova, and F. Gilardi, "Open-source large language models outperform crowd workers and approach chatgpt in text-annotation tasks," *arXiv preprint arXiv:2307.02179*, vol. 101, 2023.
- [34] M. Li, T. Shi, C. Ziems, M.-Y. Kan, N. Chen, Z. Liu, and D. Yang, "Coannotating: Uncertainty-guided work allocation between human and large language models for data annotation," in *Proceedings of the 2023 Conference on Empirical Methods in Natural Language Processing*, 2023, pp. 1487–1505.
- [35] H. Liu, C. Li, Q. Wu, and Y. J. Lee, "Visual instruction tuning," *Advances in neural information processing systems*, vol. 36, pp. 34892–34916, 2023.
- [36] X. Lu, B. Wang, X. Zheng, and X. Li, "Exploring models and data for remote sensing image caption generation," *IEEE Transactions on Geoscience and Remote Sensing*, vol. 56, no. 4, pp. 2183–2195, 2017.
- [37] Y. Mei, Y. Yang, L. Guo, Q. Wang, M.-M. Yu, X. He, W. Wu, and J. Liu, "Urbannav: Learning language-guided urban navigation from web-scale human trajectories," *arXiv preprint arXiv:2512.09607*, 2025.
- [38] C. Xie, H. Gao, Y. Huang, Z. Xue, C. Xu, and K. Dai, "Leveraging the deepseek large model: A framework for ai-assisted disaster prevention, mitigation, and emergency response systems," *Earthquake Research Advances*, p. 100378, 2025.
- [39] A. Hurst, A. Lerer, A. P. Goucher, A. Perelman, A. Ramesh, A. Clark, A. Ostrow, A. Welihinda, A. Hayes, A. Radford *et al.*, "Gpt-4o system card," *arXiv preprint arXiv:2410.21276*, 2024.
- [40] Y. Shi, X. Yu, L. Liu, T. Zhang, and H. Li, "Optimal feature transport for cross-view image geo-localization," in *Proceedings of the AAAI Conference on Artificial Intelligence*, vol. 34, no. 07, 2020, pp. 11990–11997.
- [41] Y. Shi, X. Yu, D. Campbell, and H. Li, "Where am i looking at? joint location and orientation estimation by cross-view matching," in *Proceedings of the IEEE/CVF Conference on Computer Vision and Pattern Recognition*, 2020, pp. 4064–4072.
- [42] S. Hu, M. Feng, R. M. Nguyen, and G. H. Lee, "Cvm-net: Cross-view matching network for image-based ground-to-aerial geo-localization," in *Proceedings of the IEEE Conference on Computer Vision and Pattern Recognition*, 2018, pp. 7258–7267.
- [43] H. Yang, X. Lu, and Y. Zhu, "Cross-view geo-localization with layer-to-layer transformer," *Advances in Neural Information Processing Systems*, vol. 34, pp. 29009–29020, 2021.
- [44] G. Zheng, J. Guan, M. Xie, X. Zhao, C. Fan, S. Zhang, and P. Feng, "Dual-level progressive hardness-aware reweighting for cross-view geo-localization," *arXiv preprint arXiv:2510.27181*, 2025.
- [45] Z. Lv, J. Ye, J. Yu, and W. Li, "Cross-view image geo-localization based on an improved bev transformation method," in *IGARSS 2025-IEEE International Geoscience and Remote Sensing Symposium*. IEEE, 2025, pp. 6301–6305.
- [46] J. Li, D. Li, S. Savarese, and S. Hoi, "Blip-2: Bootstrapping language-image pre-training with frozen image encoders and large language models," in *International conference on machine learning*. PMLR, 2023, pp. 19730–19742.
- [47] L. Xue, M. Shu, A. Awadalla, J. Wang, A. Yan, S. Purushwalkam, H. Zhou, V. Prabhu, Y. Dai, M. S. Ryoo *et al.*, "xgen-mm (blip-3): A family of open large multimodal models," *arXiv preprint arXiv:2408.08872*, 2024.
- [48] X. Zhai, B. Mustafa, A. Kolesnikov, and L. Beyer, "Sigmoid loss for language image pre-training," in *Proceedings of the IEEE/CVF international conference on computer vision*, 2023, pp. 11975–11986.
- [49] C. Jia, Y. Yang, Y. Xia, Y.-T. Chen, Z. Parekh, H. Pham, Q. Le, Y.-H. Sung, Z. Li, and T. Duerig, "Scaling up visual and vision-language representation learning with noisy text supervision," in *International conference on machine learning*. PMLR, 2021, pp. 4904–4916.

- [50] Y. Zeng, X. Zhang, and H. Li, “Multi-grained vision language pre-training: Aligning texts with visual concepts,” in *International Conference on Machine Learning*. PMLR, 2022, pp. 25 994–26 009.
- [51] Y. Zeng, X. Zhang, H. Li, J. Wang, J. Zhang, and W. Zhou, “ X^2 -VLM: All-in-one pre-trained model for vision-language tasks,” *IEEE transactions on pattern analysis and machine intelligence*, vol. 46, no. 5, pp. 3156–3168, 2023.
- [52] D. Hong, L. Gao, N. Yokoya, J. Yao, J. Chanussot, Q. Du, and B. Zhang, “More diverse means better: Multimodal deep learning meets remote-sensing imagery classification,” *IEEE Transactions on Geoscience and Remote Sensing*, vol. 59, no. 5, pp. 4340–4354, 2020.
- [53] K. Nogueira, O. A. Penatti, and J. A. Dos Santos, “Towards better exploiting convolutional neural networks for remote sensing scene classification,” *Pattern Recognition*, vol. 61, pp. 539–556, 2017.
- [54] M. J. Swain and D. H. Ballard, “Color indexing,” *International journal of computer vision*, vol. 7, no. 1, pp. 11–32, 1991.
- [55] N. Dalal and B. Triggs, “Histograms of oriented gradients for human detection,” in *2005 IEEE computer society conference on computer vision and pattern recognition (CVPR’05)*, vol. 1. Ieee, 2005, pp. 886–893.
- [56] J. Canny, “A computational approach to edge detection,” *IEEE Transactions on pattern analysis and machine intelligence*, no. 6, pp. 679–698, 2009.
- [57] K. He, H. Fan, Y. Wu, S. Xie, and R. Girshick, “Momentum contrast for unsupervised visual representation learning,” in *Proceedings of the IEEE/CVF conference on computer vision and pattern recognition*, 2020, pp. 9729–9738.
- [58] A. J. Wang, P. Zhou, M. Z. Shou, and S. Yan, “Enhancing visual grounding in vision-language pre-training with position-guided text prompts,” *IEEE Transactions on Pattern Analysis and Machine Intelligence*, vol. 46, no. 5, pp. 3406–3421, 2023.
- [59] A. Vaswani, N. Shazeer, N. Parmar, J. Uszkoreit, L. Jones, A. N. Gomez, Ł. Kaiser, and I. Polosukhin, “Attention is all you need,” *Advances in neural information processing systems*, vol. 30, 2017.
- [60] W. Kim, B. Son, and I. Kim, “Vilt: Vision-and-language transformer without convolution or region supervision,” in *International conference on machine learning*. PMLR, 2021, pp. 5583–5594.
- [61] Y. Xia, L. Shi, Z. Ding, J. F. Henriques, and D. Cremers, “Text2loc: 3d point cloud localization from natural language,” in *Proceedings of the IEEE/CVF conference on computer vision and pattern recognition*, 2024, pp. 14 958–14 967.
- [62] D. P. Kingma and J. Ba, “Adam: A method for stochastic optimization,” *arXiv preprint arXiv:1412.6980*, 2014.
- [63] L. McInnes, J. Healy, and J. Melville, “Umap: Uniform manifold approximation and projection for dimension reduction,” *arXiv preprint arXiv:1802.03426*, 2018.